IEEE Robotics and Automation Letters (RAL) paper presented at
2024 IEEE/RSJ International Conference on Intelligent Robots and Systems (IROS)
October 14-18, 2024. Abu Dhabi, UAE

Enhanced Optical Tracking of Weld Beads in Autonomous Inspection of Separator Vessels

Vinicius De Vargas Terres[1], Marco Antonio Simoes Teixeira[1,2], Flavio Neves-Jr[1], and Lucia Valeria Ramos de Arruda[1] and Andre Schneider de Oliveira[1]

***Abstract*—Inspection robots have been developed to support the maintenance of separator vessels. One challenge for such robots is to identify and navigate along the weld bead. This paper proposes a new solution to the weld bead recognition problem, including its tracking, which aims to automate weld bead inspection. A reliable weld bead detection method was developed through five steps that process the line profile sensor data. The weld bead was identified based on the estimation of its center. A non-linear controller paired with a module that compensates for uncertainties generated by gravity was designed to ensure the tracking of weld bead. Such a controller can reduce the impact of the variation in the robot's orientation on the weld bead tracking. An algorithm redirects the robot at the end of the weld bead. The experiments were conducted in a laboratory-scale setup, allowing movement along horizontal and diagonal surfaces. The results show that the robot tracked the weld line in all simulated conditions, with a maximum error of 2.86mm.**

***Index Terms*—Object Detection, Segmentation and Categorization, Autonomous agents, Autonomous inspection robot, Weld bead recognition, Weld bead tracking.**

I. Introduction

INSPECTION of separator vessels is required to prevent accidents that cause financial losses and environmental impacts. Strict inspection procedures are periodically executed to detect flaws. During their service life, weld beads, which are a part of the separator, require precise monitoring. Weld bead integrity evaluation is carried out using non-destructive test (NDT) methods. Ultrasonic inspection, which detects the location, size, and orientation of flaws based on ultrasound signals [1], is typically used for evaluating weld beads.

In-service inspection is a useful option for oil and gas companies. The primary benefit is the reduction in the financial loss because of downtime and the procedure for stopping and restarting equipment. However, the working temperature of the vessel presents a challenge for in-service inspection. High operating temperatures prevent access for human inspectors. One solution is to use a robotic system carrying an NDT device. Inspection robots ease access to hazardous environments and execute repetitive tasks reliably, thereby speeding up the process of inspecting equipment. The primary applications for inspection robots include the inspection of pipes [2], [3], storage tanks [4] and separator vessels [5]. The wall-climbing inspection is typically used to inspect vertical structures such as separator vessels. Magnetic inspection robots are widely used owing to their robust adhesion to metallic surfaces [6].

Ultrasonic inspection requires the sensor to run along the weld bead to operate. During autonomous inspection, the robot must track the weld bead accurately. Therefore, the robotic system must recognize the weld bead, indicate its position over the vessel, using the robot coordinates as a reference, and follow the bead along its entire length. Accurate navigation is required because the proximity between the weld bead and the ultrasound equipment. Nonetheless, accurate identification of the weld bead is difficult because of its millimetric size.

The uncertainty in the path of the robot caused by gravity during the climb is another challenge for autonomous inspection. Gravity introduces errors in the robot's movements, which causes the robot to veer from the weld bead. This effect must be corrected to ensure accurate weld bead tracking. The solutions in the literature does not provide a applied weld bead tracking method that ensures high precision needed for autonomous inspection. This work contributes developing a precise identification method that works with weld bead tracking system in different robot orientations.

The primary goal of this study is to propose a new approach to identifying and tracking weld beads for automation of the weld bead inspection. Automation is implemented using the Climbing Robot for Autonomous inSpection (CRAS) [5]. A new weld bead recognition algorithm is developed that processes the measurements of the weld bead sensed by a line profile sensor and calculates the position of the weld bead center. Additionally, we develop a non-linear controller with gravity compensation for weld bead tracking. The control system is designed to achieve the millimetric accuracy required for inspection. Furthermore, a turnaround algorithm is proposed to search for a new bead when the robot ends the tracking.

The remainder of this paper is organized as follows: Section II discusses related work. Section III details the robot CRAS. Section IV details the approach used to track the weld bead. Section V presents and discusses the results obtained. Section VI discusses an overall evaluation of the approach. Section VII concludes the analysis and suggests future works.

Manuscript received: August, 28, 2023; Accepted October, 17, 2023.

This paper was recommended for publication by Editor Markus Vincze upon evaluation of the Associate Editor and Reviewers' comments. This study was supported by the Human Resource Program of The Brazilian National Agency for Petroleum, Natural Gas, and Biofuels PRH-ANP–FINEP Management, contractual instrument n° 0.1.19.0240.00, Ref 0431/19-PRH21-UTFPR, and PETROBRÁS-5850.0105441.17.9-CRAS 3793.12483-4 grant through PETROBRAS Human Resources Training Program.

[1] All authors are with Universidade Tecnológica Federal do Paraná (UTFPR), Curitiba 80230-901, Brazil viniciusterres@utfpr.edu.br.

[2] Marco Antonio Simões Teixeira is with Pontifícia Universidade Católica do Paraná (PUCPR), Rua Imaculada Conceição, 1155 Curitiba, Brazil.

Digital Object Identifier (DOI): see top of this page.

II. Related Work

The development of autonomous inspection is hampered by the difficulty in recognizing weld beads. A typical approach is to use laser-based vision sensors to detect weld beads, as presented in [7], [8], [9], [10]. Vision-based methods have some drawbacks when compared with techniques based on line profile scanners. Their computational cost is higher owing to the need for extraction of the weld bead profile from the image [11], [12], [13], [14]. Dong *el at* [15] presented a deep learning network for extracting weld bead. The information from multiple weld boundaries is fused to obtain the weld line. However, the approaches in [15] do not provide precise localization of the bead position, but only define a bounding box around the weld line. Weld bead tracking requires the identification of the precise location of the weld bead center to command the robot's navigation correctly.

The time spent processing the bead measurement is a relevant characteristic of weld bead identification methods. The recognition must be sufficiently fast such as it does not interfere with weld bead tracking. The delay in detecting the weld bead detection causes uncertainty in the monitoring, hampering the usage of vision-based sensors.

Computer vision-based methods use filtering strategies to improve weld bead detection [16], [17]. Noise reduction provides a straightforward weld bead measurement, highlighting the reinforcement of the weld bead from the metal surface. The filtering process leads to accurate weld bead detection.

Another challenge is estimating the height, width, and center of the weld bead from the measured profile. The weld reinforcement has an irregular format, which makes it difficult to consistently achieve accurate weld bead estimation. For example, Han *et al* [18] proposed an approach for measuring the weld bead and inspecting its quality. This work shows defects that might occur in a weld bead, such as misalignment, mismatch, and undercut. These flaws prevent the usage of the highest point for estimating weld bead position.

A solution to these issues is to sense the weld bead using a line profile sensor, as in [19] and [20]. In [19], the authors used signal analysis to develop a new method for recognizing the weld bead center junctions with the parent base. However, the weld bead junction with the parent base might be blurred because of weld bead corrosion. Identification must consider other factors to implement an accurate strategy. The laser detection method is main difference between lased-based vision sensors and line profile scanner. Lased-based vision sensors acquire an image of the laser and transmit the image, while line profile sensors emit and detect laser signal and transmit the data as a scan or a point cloud.

There are several types of control algorithms for tracking weld beads [21], [22], [19], [23]. For example, a platform with two degrees of freedom was designed to maintain the position at the desired accuracy using a semi-closed-loop motion control method by Zhu *et al*[19]. Nonetheless, the approaches cited do not handle the gravity effect on tracking, which is essential for accurate tracking of the weld bead.

In a previous work, we presented methods to implement a weld bead tracking controller [24]. However, the effect of gravity on controller performance was simulated. The current study analyzes this influence using a testing laboratory-scale apparatus and is, therefore, closer to real-life situations. The dependence on the shape of the weld bead to identify the weld bead used to identify it is another issue addressed in this study. Therefore, this study presents a more generic solution.

III. Climbing Robot For Autonomous InSpection

This section describes the robot selected for the automated inspection using the proposed weld bead identification and tracking algorithm. The CRAS, is shown in Figure 1a. It is a climbing robot designed to inspect weld beads on industrial super-duplex steel vessels. The surface to be inspected is at a high temperature (defined here as ranging from 80ºC to 135ºC), as observed in the thermal image in Figure 1b.

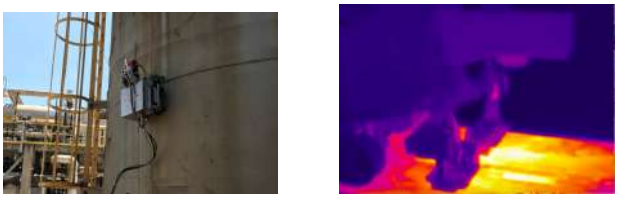

(a) Climbing (b) Inspecting

Fig. 1: CRAS working in Petroquimecal plants.

CRAS was developed by the Automation and Advanced Control System Laboratory at the Federal University of Technology - Paraná. It is an evolution of an older generation of robot, called Autonomous Inspection Robot [25], [26]. The robot has four independent directional magnetic wheels, as shown in Figure 2. Each wheel has a module of two servomotors. The module comprises one motor for steering the wheel and the another motor for driving the robot. Detailed information about the robot can be found in [5] and [27].

The inspection technique used to inspect the weld beads is phased-array ultrasound non-destructive testing. Two high-temperature wedges collect data from the weld bead. The ultrasonic wedges support position is set by a threaded spindle, which rises during navigation and lowers during inspection.

The robot uses three sources of perception for interacting with the environment. The first is a Leuze LRS36/6 sensor that measures the weld bead. This sensor is a profile scanner with a minimum object size of 1 mm at a Z distance of 200 mm. The maximum number of sample points is 376, quantized at 0.1

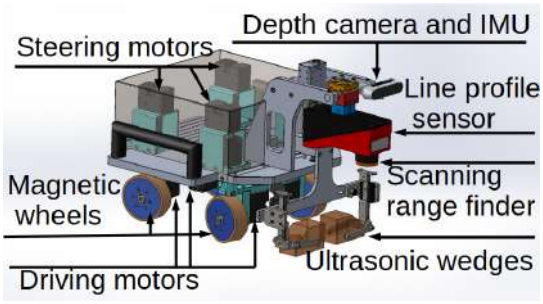

Fig. 2: Climbing Robot for Autonomous InSpection. [27]

mm forming a cloud of 2D points. Each point is the position in the x and z direction. The second is a scanning range finder that detects obstacles in the robot's navigation path. The third is a depth camera integrated with an inertial measurement unit (IMU), which carries out the inertial measurement of the robot and the perception of the front of the robot. Moreover, the camera enables remote navigation by the operator.

IV. Enhanced Tracking of Weld beads

This section describes the development of proposed approach for implementing weld tracking by the robot. This tracking is performed in three steps, beginning with weld bead recognition. The goal of the first step is to identify the weld bead and calculate the alignment error and the distance of the weld bead center from the robot alignment center. The second step involves the robot control system, which is responsible for tracking the bead based on the response of the recognition. The third step is the turnaround algorithm, whose function is to redirect the robot after the end of a weld bead inspection.

A. Recognition of Weld beads

Weld bead recognition is essential for the robot to determine the weld bead position and to track it successfully in the environment. A flow chart of the weld bead recognition algorithm is shown in Figure 3. The input to this algorithm, which has been developed in this study, is measurements of the line profile sensor stored in a 2D point cloud database. The outputs are the presence of a weld bead at the signal measured by the sensor and the position of the weld bead center. The line profile sensor reference system has two axes. The x-axis represents the distance from the laser center. The z-axis represents the height.

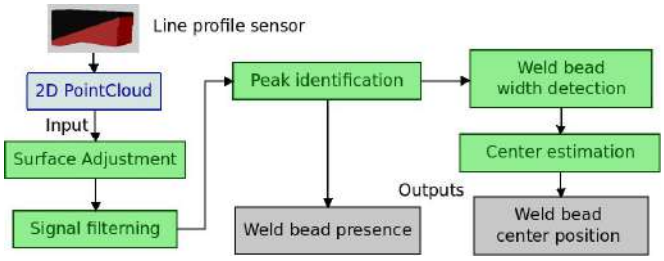

Fig. 3: Flow chart of the weld bead recognition procedure.

Surface compensation, the first step, minimize the effects of the environmental surface on the weld bead measurement. The method estimates the metal base position without the weld bead and subtracts the estimate from raw signal. Initially, a window is separated from the signal, representing the region where weld bead is placed. The window starts at -16mm and stop at 16mm. The remaining signal is grouped into two data sets. The first group encompasses the signal points to the left of the window and the second group includes the data to the right of the window. The two groups of signals have data only from metal base, allowing the isolation of the weld bead.

For each group, a linear regression procedure is used to estimate the surface effects. Equation 1 provides the linear function used for the regression, where a is the angular coefficient, b is the linear coefficient, x is the independent variable, and y is the dependent variable.

$$y = ax + b \tag{1}$$

The final estimate of the surface is the average of the left and right estimators. This surface estimation is subtracted from the complete signal, including the center window. Figures 4a and 4b show the measured signals before and after the surface compensation procedure. The blue dots represent the weld bead, and the green dots represent the metal base of the weld bead. It is possible to observe that the module transformed the signal to let the weld bead peak upside and the metal base near to zero, easing the recognition.

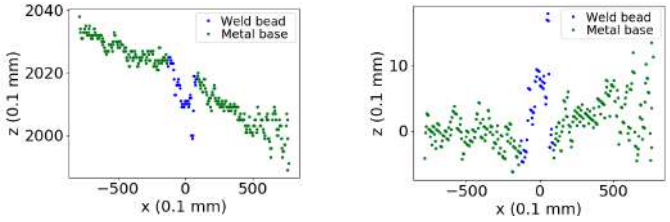

(a) Raw signal of a weld bead. (b) Signal after the first step.

Fig. 4: Weld bead signals during the surface estimation.

It is worth noting that the performance of the surface compensation procedure depends on the function used in the regression. We can use a quadratic or linear function according to the environmental surface characteristics (concave, convex, or flat). However, mean value estimation is not recommended. The mean value can hinder the identification of the weld bead because this estimation would not capture the surface effects in the horizontal direction when the robot's wheels pass by an obstacle, as shown in Figure 4a.

The next step, based on the flow chart in Figure 3, is signal filtering. The filtering technique is the Surface Estimation via Analysis Method (SEAM) proposed by Moura *et al* (2021). [28]. The technique was originally developed for estimation with ultrasound signal profiles. Because the main requirement for SEAM applications is that the signal must be piecewise linear, the method is useful for the weld bead signal as measured in this study. The SEAM is a variation of the total variation seminorm filter with regularization, whose primary advantage is its ability to cope with non-linear signal regions. In addition, the distortion of the edges is reduced.

The third step is peak identification. The local maximum values of the signal and its positions are calculated. These are candidates for the weld bead peak. The initial candidate is the maximum value with the highest height until the lowest contour line. If the candidate is lower than the sensor resolution, the signal does not have a bead. In this case, the algorithm stops and flags the absence of a bead to the control system.

When a candidate satisfies the resolution condition, its distance from the last center is computed. If the distance between the current peak and the previous center is lower than a empirically set fixed value, the candidate is the weld bead peak. If not, the candidate is eliminated, and a new candidate is evaluated until the peak of the weld bead is found.

The fourth step is weld bead width detection. The primary objective of this section is to determine an estimation of the weld bead center. Weld bead limits are established at six positions, at percentages of the height of the bead, starting with the highest value of the bead. The positions are 30%, 40%, 50%, 60%, 70% and 80% of the height of the bead.

A horizontal line is drawn in these positions. The initial value of the weld bead limits corresponds to the intersection point between the lines and the signal, as illustrated by Figure 5. The blue dots, the green dots, orange line, the dashed red line, the red dots, the black dots represent the weld bead, the metal base, the height of the weld bead, the width of the weld bead, the weld bead limit and the weld bead center for each position of the weld bead limits.

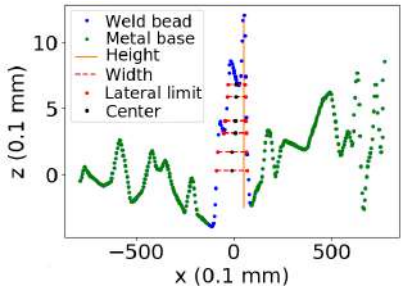

Fig. 5: Signal during the calculus of the weld bead center.

The presence of secondary peaks in the weld bead is tested for each position. A secondary peak is the maximum local value near the current maximum. The distance in the x-direction between the local maximum and the initial value of the weld bead is calculated. If this distance is smaller than the threshold value, the weld bead limit is expanded based on the presence of the secondary peak. The mean value of the weld limits is the center position value. The center value with the shortest distance to the last weld bead center is determined as the weld bead center of the measurement.

The fifth step is the weld bead center estimation. This module obtains the output from the weld bead width detection as input and determines the center position corresponding to the mean value of the last five center positions. Calculating the mean of more than five points mitigates the noise that might arise from with the weld bead format variation. Finally, the result is considered the weld bead center position.

B. Motion Control

The tracking of a weld bead is required for its inspection. The robot must move parallel to the weld bead, aligning its center with the weld bead center. Therefore, the robot's control must compensate for alignment errors while navigating.

Figure 6 illustrates four blocks of the system proposed in this study. A weld bead line track controller implements initial control of weld bead tracking. Gravity compensation compensates for the effects of gravity. A turnaround algorithm is an algorithm that searches for weld beads, and is executed when the bead is not found. A switch is used to change between the turnaround algorithm and the weld bead line controller. The control system outputs are the steering angle and drive speed. The steering angle sets the direction of each wheel, and the driving speed indicates the speed for the robot.

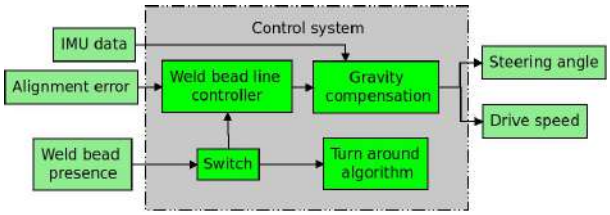

Fig. 6: Representation of the control system.

The switch analyzes the weld bead presence input in the signal and activates the corresponding part. The weld bead line controller is activated when the measured signal contains a weld bead, while the turnaround algorithm is activated when a weld bead is not found.

The weld bead line tracking controller is a non-linear single-input single-output (SISO) controller based on a sigmoid function. A benefit of this study is the low computational cost of such a control function. The input to the controller is the alignment error, while the controlled output is the alignment angle, which is an early estimate of the steering angle. The value used as the alignment error is the weld bead center position. The usage of a non-linear controller improves the controller performance when compared to a linear controller. This happens because of the smoother transition between upper and lower bounds, allowing a better adjustment of the robot. Equation 2 models the control law between the alignment error and the alignment angle, where AE is the alignment error, and AA is the alignment angle. The parameters of the sigmoid function are defined based on empirical tests.

$$AA = -0.1485 + 0.3((1 + e^{(-(AE-0.09))/4.7})^{-1} \quad (2)$$

The alignment angle from the weld bead line controller and the linear acceleration, which is approximately the acceleration caused by gravity, are inputs to the gravity compensation. The module sets the steering angle and drive speed of the motors. The motors define the drive speed as a fixed value of 10.43 mm/s. This value represents the speed required by the ultrasound system. The steering angle is the sum between the alignment angle and the gravity correction angle.

Equation 3 shows the gravity correction angle, where α is the gravity correction angle, β is the maximum correction angle, which is -0.0486 rad and a_x, a_y, and a_z are the linear acceleration measured by the IMU in the x, y and z directions. The value $a_y/\sqrt{(a_x^2 + a_y^2 + a_z^2)}$ establishes a metric to calculate the influence of lateral acceleration on the robot. The fraction returns a dimensionless value equivalent to the sine of the robot's roll angle. As the robot is tilted, the robot's roll angle rises, as the gravity compensation angle.

$$\alpha = \beta * a_y/\sqrt{(a_x^2 + a_y^2 + a_z^2)} \quad (3)$$

C. Turnaround approach

The turnaround algorithm redirects the robot when the weld bead track is complete. The search for a new weld bead runs in

an orientation orthogonal to that of the old bead. The operator defines the side to which the robot turns. The algorithm begins when no bead is detected. Initially, the robot aligns the wheels at 0º. The next step is to move the robot forward by activating the drive motors at 10.43 mm/s. The travel distance is from the line profile sensor to the center of the robot. The encoder of the motor estimates the travel distance. The next step redirects the wheels to a position that allows the robot to rotate over the z-axis. The robot subsequently turns over the z-axis and moves its orientation to the new bead to be analyzed. The final step is the robot's return to the beginning of the new weld bead.

V. Experimental results and evaluation

This section discusses the results obtained for the weld bead tracking system. The system was tested using three elements. The first element was the weld bead recognition algorithm test, which tested the proposal, validating the algorithm used to detect the weld bead. The second element tested was the control system, for which the experiments evaluated the influence of gravity on weld bead tracking. The third element was the execution of the turnaround algorithm.

A. Real laboratory-scale apparatus

A laboratory-scale apparatus containing weld beads as industrial vessels was used to evaluate the developed system. It comprised a metallic support and a metal plate 22 mm thick. The inner part of the plate was a compound of duplex steel, and the outer part was a compound of super duplex steel. Some differences between super duplex and carbon steel were the reduction in the magnetic adhesion and the increase in corrosion resistance. The support allows posing the plate to be placed in eight positions: two vertical, two horizontal, and four diagonal at an angle of 45 degrees. The plate contained 36 sections of weld beads with 24 intersections among them. The average height of the weld bead was approximately two millimeters. Figure 7 illustrates the testing device [27].

(a) Plate in vertical position (b) Plate at -45 degrees

Fig. 7: Apparatus with plate used in the tests

B. Weld bead recognition analysis

This experiment aimed to examine the weld bead tracking performance. Its primary focus was to validate the proposed algorithm to identify the weld bead. Initially, the robot was positioned at the beginning of the weld bead with the robot alignment center placed close to the weld bead center, as shown in Figure 9a. The robot had to track a straight section of a weld bead until the end, approximately 15 cm away.

A five-step test was used to evaluate the impact of each module on weld bead recognition. The step-by-step test provided a detailed analysis of the functioning of the weld bead, one for each weld bead recognition module. As the peak identification determines the highest point of the weld bead, it was defined as the first step because the module provides an initial estimate of the weld bead. The other modules followed the algorithm as shown in Figure 3. The experiment was repeated ten times for each step. The modules present in each step are as follows:

- P1: Peak identification.
- P2: Peak identification and surface compensation.
- P3: Peak identification, surface compensation and signal filtering.
- P4: Peak identification, surface compensation, signal filtering and weld bead width detection.
- P5: Complete algorithm

The experiment showed that the robot was able to execute precise tracking of the weld bead using the proposed approach. Figure 8a shows the alignment error module distribution over the recognition algorithm. When additional modules were used in the recognition algorithm, the alignment error and its variations were reduced. This reduction indicates a greater accuracy in the detection of the weld bead center.

Table I lists the results obtained for the mean value, accuracy and maximum value of the alignment error module. The standard deviation of the alignment error module at each repetition of the weld bead tracking was considered a metric for evaluating the accuracy of navigation along the weld bead. The accuracy was calculated as the mean value of the alignment error module standard deviation for each repetition of the weld bead tracking. The overall improvement of the alignment error module was 72.61%.

Figure 8b shows the steering angle distribution over the recognition algorithm. It is worth mentioning that the steering angle decreased its range when using a more complete approach. Table II lists the results obtained for the absolute maximum value of the steering angle. The absolute maximum value of the steering angle decreases when more modules were used in the weld bead identification, as observed in Table II. This indicates a smoother action by the controller, which is a signal of improvements caused by the proposed algorithm.

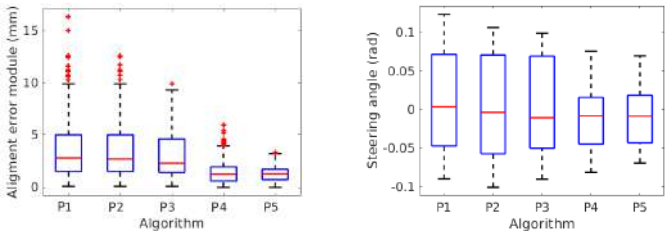

(a) (b)

Fig. 8: Boxplot representing (a) alignment error module and (b) steering angle over weld bead recognition experiment.

These results allow us to conclude that each step of the weld bead recognition system reduced the tracking error. One major observation is that P4 had the most impressive improvement in

TABLE I: Results of recognition analysis considering accuracy, mean and maximum value of alignment error module.

	Mean Error (mm)	Standard deviation	Improvement (%)	Accuracy (mm)	Standard deviation	Improvement (%)	Maximum error (mm)	Standard deviation	Improvement (%)
P1	3.55	0.49	-	2.39	0.23	-	11.8	2.39	-
P2	3.47	0.35	2.25	2.42	0.23	-	11.6	2.09	1.69
P3	3.28	0.84	7.60	2.06	0.26	8.78	8.06	0.85	31.78
P4	1.41	0.28	60.35	0.97	0.26	59,41	4.32	1.08	63.33
P5	1.22	0.20	65.39	0.63	0.13	73.06	2.47	0.45	79.09

TABLE II: Results of recognition analysis considering the absolute maximum value of the steering angle

	Absolute maximum error (rad)	Standard deviation (rad)	Improvement(%)
P1	0,1239	0.0086	
P2	0,1066	0.0083	13,96
P3	0,0993	0.0081	19,85
P4	0,0746	0.0046	39,79
P5	0,0657	0.0052	46,97

error. In this step, the correction of weld bead width mitigated the effect on the weld bead center calculation owing to changes in the reinforcement format of the weld bead. The entire weld bead recognition system configured a data processing technique that improved the extraction of the weld bead center.

C. Gravity influence analysis

A robot that tracks the weld bead over a vessel must navigate under different climbing conditions. The gravity analysis experiment evaluated the system performance under several gravity effects caused by the climbing conditions. Two groups of experiments were carried out. The first examined the robot's action with x-axis gravity variations, while the second investigated the robot's motion with y-axis gravity variations.

The experiments were conducted on two straight sections of the apparatus. The gravity force variation is obtained by placing the plate in diagonal positions. Initially, the robot was placed at the beginning of the weld bead with the robot alignment center close to the bead center, as shown in Figure 9a. It was tasked with tracking the 15 cm section until the end.

Six setups were simulated, emulating the diverse conditions that the robot can encounter during weld bead tracking and inspection. The robot had to maintain the weld bead tracking under all conditions. The experiment was repeated ten times for each setup. Figure 9 illustrates the robot's position in each setup. The setups are described as follows:

- Setup 1: No gravity action on the x-axis, the robot navigates a ground surface, as shown in Figure 9a
- Setup 2: No gravity action on the y-axis, the robot navigates a ground surface, as shown in Figure 9b
- Setup 3: The robot is climbing at 45º, as shown in Figure 9c
- Setup 4: The robot experiences the influence of gravity on the left side, as shown in Figure 9d.
- Setup 5: The robot is descending at 45º, as shown in Figure 9e
- Setup 6: The robot experiences the influence of gravity on the right side, as shown in Figure 9f

(a) 1: reference for x-axis

(b) 2: reference for y-axis

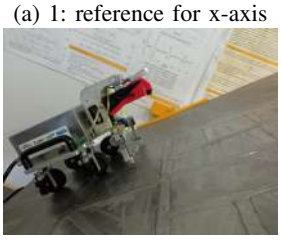

(c) 3: climbing at 45º

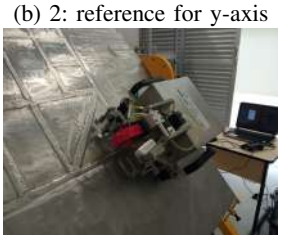

(d) 4: left side at 45º

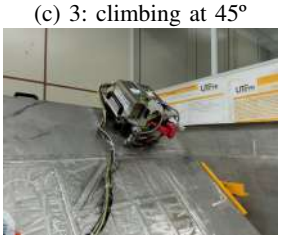

(e) 5: descending at 45º

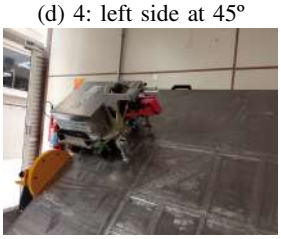

(f) 6: right side at 45º

Fig. 9: Setups for the gravity influence analysis experiments

The setups considered for the evaluation of the impact of the increase in x-axis component of the gravity force were setups 1, 3, and 5, representing the robot's pitch movement. Figures 10a and 10b display the results of the mean value of the absolute alignment error and the steering angle on the x-axis for each setup, respectively. From these figures, it was found that the x-axis component variation of the gravity force caused the robot to move in a zig-zag manner owing to the decrease in the normal force intensity. In-ground navigation (setup 1), gravity did not affect the alignment error. For climbing (setup 3) and descending (setup 5), the gravity force induced an error, observed in the higher variations of the alignment error absolute value and the steering angle. Despite this, the controller overcame such situations and maintained the mean value of the alignment error at an absolute value above 2 mm.

The setups considered for the valuation of the impact of the increase in y-axis component of the gravity force were setups 2, 4, and 6, representing the robot's roll movement. Figures 11a and 11b show the mean values of the absolute alignment error and steering angle on the y-axis for each setup, respectively. The action of the gravity compensation module can be observed. Owing to the gravity effect, the

TABLE III: Overall analysis of the proposed approach.

	Mean error (mm)	Standard deviation	Accuracy (mm)	Standard deviation	Maximum error (mm)	Standard deviation
Setup 1	1.06	0.28	0.73	0.23	2.54	0.72
Setup 2	1.34	0.43	0.76	0.23	2.99	0.59
Setup 3	1.34	0.33	0.77	0.26	2.84	0.60
Setup 4	1.49	0.31	0.85	0.26	3.04	0.61
Setup 5	1.32	0.41	0.77	0.13	2.93	0.52
Setup 6	1.32	0.47	0.79	0.23	2.85	0.62
Overall	**1.31**	**0.37**	**0,78**	**0.22**	**2.86**	**0.61**

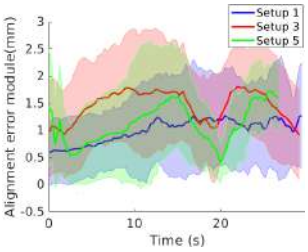

(a) Alignment error absolute value over time.

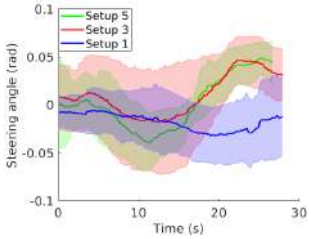

(b) Steering angle over time.

Fig. 10: Mean value of the results for 10 experiments, considering x-axis impact.

(a) Robot executing the turnaround procedure.

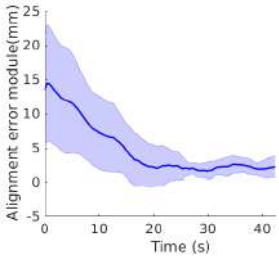

(b) Alignment error after the redirection.

Fig. 12: Turnaround execution results.

robot tended to slip on the y-axis, shifting the robot from the weld bead center. In setup 4, the robot slid to the left, requiring a right-side correction. In setup 6, the robot slid to the right, necessitating a left-side compensation. This slippage implies implies a module of steering angle value for the same alignment error value, as shown in Figures 11a and 11b.

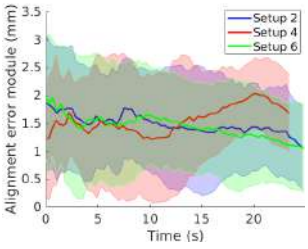

(a) Alignment error absolute value over time.

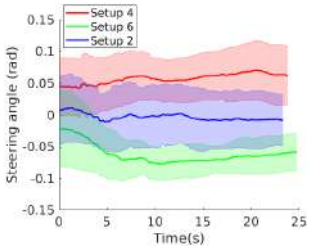

(b) Steering angle over time.

Fig. 11: Mean value of the results for 10 experiments, considering the y-axis impact.

D. Turnaround algorithm evaluation

This experiment was designed to analyze the alignment error after the turnaround procedure. The experiment demonstrated the operation when a weld bead is not found. The robot was placed in a weld bead section over the apparatus. The turnaround algorithm redirected the robot to a new bead. The old and the new weld bead were orthogonal. The experiment was repeated ten times. Figure 12a shows the initial position.

Figure 12b shows the absolute value of the alignment error during the turnaround procedure which searches for the beginning of the new weld bead. The redirection of the robot increased the alignment error at the initial time instants. This increase occurred when the robot's wheel passed through a weld bead, looking for its center. The curve shows an exponential decrease until the error reaches a steady value. The mean and maximum values of the alignment error at the end of the turnaround algorithm were 1.81 and 3.02 mm.

VI. Overall System Evaluation

Three sets of experiments were conducted to evaluate the proposed weld bead tracking control over a testing device that simulated the conditions of a separator vessel. The experiments examined the weld bead recognition algorithm, the effect of gravity on weld bead tracking considering variations in x-axis and y-axis, and the execution of turns.

Table III lists the results of the experiments conducted in Section V. The accuracy was calculated as the standard deviation for single weld bead tracking. This metric evaluated the alignment error variation during each experiment.

Gravity affected the weld bead tracking performance, increasing the alignment error mean value compared with the first experiment. However, the robot was tested in situations that emulated the separator vessel and could overcome the changes in orientation and execute the corrections required for precise weld bead tracking, as listed in Table III.

This study presents an upgrade of the processing techniques for weld bead tracking. The overall improvement of the weld bead tracking, compared with the weld bead identification from the raw data, was 72,61%, as commented in subsection V-B. The weld bead tracking reached an error close to the line profile sensor accuracy of approximately 1 mm.

The results obtained in this study can be compared to those of our previous work [24]. A previous study presented a weld bead tracking strategy based on a weld bead algorithm and a fuzzy controller. The maximum error obtained was 3 mm. The recognized weld bead profile was smaller and had a more variable format. In addition, the tracking validation included

tests with different robot orientations. Despite the differences between the two works, the current weld bead recognition and tracking system outperformed the earlier method by 0.14mm.

VII. Conclusion

This study discussed a new technique to recognize and navigate along weld beads, focusing on providing an accurate and robust method for robot orientation changes. A line profile sensor and an IMU were used to measure the weld bead and the effect of gravity. The identification was based on a five-step algorithm that analyzed data from the laser profile scanner. The control of the robot was based on a controller associated with a gravity compensation system. An algorithm was developed to turn the robot at the end of a weld bead section.

The results showed that the proposed method is robust with respect to the robot's orientation change. The algorithm improved the identification of the weld bead until it approached the line profile sensor accuracy. The control compensated for the effects of gravity on the robot, allowing for effective weld bead tracking. The maximum and mean error of the alignment were 2.86 and 1.31 mm, respectively.

Future works will consider new techniques that improve the calculation of weld bead parameters, the detection of weld beads, and the control of the robot. Adding new sensors is an alternative to provide a wide view of the weld bead.

References

[1] W. Fan, D. Wan, Z. Xu, Y. Wang, and H. Du, "Feature extraction of echo signal of weld defect guided waves based on sparse representation," *IEEE Sensors Journal*, vol. 20, no. 5, pp. 2692–2700, 2019.

[2] D. Xie, J. Liu, R. Kang, and S. Zuo, "Fully 3d-printed modular pipe-climbing robot," *IEEE Robotics and Automation Letters*, vol. 6, no. 2, pp. 462–469, 2021.

[3] H. Hu, K. Zhang, A. H. Tan, M. Ruan, C. Agia, and G. Nejat, "A sim-to-real pipeline for deep reinforcement learning for autonomous robot navigation in cluttered rough terrain," *IEEE Robotics and Automation Letters*, vol. 6, no. 4, pp. 6569–6576, 2021.

[4] K. Thung-Od, K. Kanjanawanishkul, T. Maneewarn, T. Sethaput, and A. Boonyaprapasorn, "An in-pipe inspection robot with permanent magnets and omnidirectional wheels: Design and implementation," *Applied Sciences*, vol. 12, no. 3, p. 1226, 2022.

[5] N. Dalmedico, H. B. Santos, J. S. Slongo, M. A. S. Teixeira, P. S. Palar, V. V. Terres, A. S. d. Oliveira, L. V. R. d. Arruda, F. Neves Júnior, and J. E. Ramos, "Cras (climbing robot for autonomous inspection): The challenges of a high-temperature tank," in *Iberian Robotics conference*. Springer, 2019, pp. 327–338.

[6] O.-L. Ouabi, P. Pomarede, M. Geist, N. F. Declercq, and C. Pradalier, "A fastslam approach integrating beamforming maps for ultrasound-based robotic inspection of metal structures," *IEEE Robotics and Automation Letters*, vol. 6, no. 2, pp. 2908–2913, 2021.

[7] H. N. M. Shah, M. Sulaiman, A. Z. Shukor, Z. Kamis, and A. A. Rahman, "Butt welding joints recognition and location identification by using local thresholding," *Robotics and Computer-Integrated Manufacturing*, vol. 51, pp. 181–188, 6 2018.

[8] J. Fan, F. Jing, L. Yang, L. Teng, and M. Tan, "A precise initial weld point guiding method of micro-gap weld based on structured light vision sensor," *IEEE Sensors Journal*, vol. 19, no. 1, pp. 322–331, 2018.

[9] R. Xiao, Y. Xu, Z. Hou, C. Chen, and S. Chen, "An adaptive feature extraction algorithm for multiple typical seam tracking based on vision sensor in robotic arc welding," *Sensors and Actuators, A: Physical*, vol. 297, p. 111533, 2019.

[10] P. Zhou, R. Peng, M. Xu, V. Wu, and D. Navarro-Alarcon, "Path planning with automatic seam extraction over point cloud models for robotic arc welding," *IEEE Robotics and Automation Letters*, vol. 6, no. 3, pp. 5002–5009, 2021.

[11] L. Yang, E. Li, T. Long, J. Fan, and Z. Liang, "A novel 3-d path extraction method for arc welding robot based on stereo structured light sensor," *IEEE Sensors Journal*, vol. 19, no. 2, pp. 763–773, 2018.

[12] ——, "A high-speed seam extraction method based on the novel structured-light sensor for arc welding robot: A review," *IEEE Sensors Journal*, vol. 18, no. 21, pp. 8631–8641, 2018.

[13] Z. Lu, J. Fan, Z. Hou, S. Deng, C. Zhou, and F. Jing, "Automatic 3d seam extraction method for welding robot based on monocular structured light," *IEEE Sensors Journal*, vol. 21, no. 14, pp. 16 359–16 370, 2021.

[14] L. Yang, J. Fan, Y. Liu, E. Li, J. Peng, and Z. Liang, "Automatic Detection and Location of Weld Beads With Deep Convolutional Neural Networks," *IEEE Transactions on Instrumentation and Measurement*, vol. 70, p. 5001912, 2021.

[15] Z. Dong, Z. Mai, S. Yin, J. Wang, J. Yuan, and Y. Fei, "A weld line detection robot based on structure light for automatic ndt," *The International Journal of Advanced Manufacturing Technology*, vol. 111, pp. 1831–1845, 2020.

[16] L. Yang, J. Fan, B. Huo, E. Li, and Y. Liu, "Image denoising of seam images with deep learning for laser vision seam tracking," *IEEE Sensors Journal*, vol. 22, no. 6, pp. 6098–6107, 2022.

[17] N. Wang, K. Zhong, X. Shi, and X. Zhang, "A robust weld seam recognition method under heavy noise based on structured-light vision," *Robotics and Computer-Integrated Manufacturing*, vol. 61, p. 101821, 2 2020.

[18] Y. Han, J. Fan, and X. Yang, "A structured light vision sensor for on-line weld bead measurement and weld quality inspection," *International Journal of Advanced Manufacturing Technology*, vol. 106, no. 5-6, pp. 2065–2078, jan 2020.

[19] Y. Zhu, X. He, Q. Liu, and W. Guo, "Semiclosed-loop motion control with robust weld bead tracking for a spiral seam weld beads grinding robot," *Robotics and Computer-Integrated Manufacturing*, vol. 73, p. 102254, feb 2022.

[20] G. Ye, J. Guo, Z. Sun, C. Li, and S. Zhong, "Weld bead recognition using laser vision with model-based classification," *Robotics and Computer-Integrated Manufacturing*, vol. 52, no. February, pp. 9–16, 2018.

[21] X. Lü, K. Zhang, and Y. Wu, "The seam position detection and tracking for the mobile welding robot," *The International Journal of Advanced Manufacturing Technology*, vol. 88, no. 5-8, pp. 2201–2210, 2017.

[22] O. Kermorgant, "A magnetic climbing robot to perform autonomous welding in the shipbuilding industry," *Robotics and Computer-Integrated Manufacturing*, vol. 53, pp. 178–186, 2018.

[23] Y. Tao, F. Ren, J. Yang, T. Wang, C. Chen, and S. Jiang, "A robot method based on self-adjusting factor fuzzy control algorithm for the seam tracking," in *2019 IEEE International Conference on Robotics and Biomimetics (ROBIO)*. IEEE, 2019, pp. 1001–1006.

[24] V. de Vargas Terres, A. S. de Oliveira, H. B. Santos, L. V. R. de Arruda, F. Neves, J. A. Fabro, and J. E. Ramos, "Rigorous tracking of weld beads for the autonomous inspection with a climbing robot," in *2019 Latin American Robotics Symposium (LARS), 2019 Brazilian Symposium on Robotics (SBR) and 2019 Workshop on Robotics in Education (WRE)*. IEEE, 2019, pp. 252–257.

[25] H. B. Santos, M. A. S. Teixeira, A. S. de Oliveira, L. V. R. de Arruda, and F. Neves-Jr, "Quasi-omnidirectional fuzzy control of a climbing robot for inspection tasks," *Journal of Intelligent & Robotic Systems*, vol. 91, pp. 333–347, 2018.

[26] M. A. S. Teixeira, H. B. Santos, N. Dalmedico, L. V. R. de Arruda, A. S. de Oliveira *et al.*, "Intelligent environment recognition and prediction for ndt inspection through autonomous climbing robot," *Journal of Intelligent & Robotic Systems*, vol. 92, no. 2, pp. 323–342, 2018.

[27] G. F. Ventura and L. Dias, "Desenvolvimento de projeto e protótipo de robô compacto para inspeção de juntas soldadas em superfícies metálicas verticais," B.S. Thesis, Federal University of Technology - Paraná, Curitiba, Brazil, 2020.

[28] H. L. de Moura, T. d. Almeida Prado, G. A. Guarneri, T. A. R. Passarin, D. Rossato, G. P. Pires, and D. R. Pipa, "Surface estimation via analysis method: A constrained inverse problem approach," *IEEE Transactions on Ultrasonics, Ferroelectrics, and Frequency Control*, vol. 68, no. 11, pp. 3386–3395, 2021.